Journal for ImmunoTherapy of Cancer

Preclinical evaluation of antigen-sensitive B7-H3-targeting nanobody-based CAR-T cells in glioblastoma cautions for on-target, off-tumor toxicity

Fien Meeus ,[1,2] Cyprine Neba Funeh,[2] Robin Maximilian Awad,[1] Katty Zeven,[2] Dorien Autaers,[1] Ann De Becker,[3] Ivan Van Riet,[3,4] Cleo Goyvaerts ,[2] Sandra Tuyaerts ,[5,6] Bart Neyns,[5,6] Nick Devoogdt ,[2] Yannick De Vlaeminck,[1] Karine Breckpot[1]

To cite: Meeus F, Funeh CN, Awad RM, *et al*. Preclinical evaluation of antigen-sensitive B7-H3-targeting nanobody-based CAR-T cells in glioblastoma cautions for on-target, off-tumor toxicity. *Journal for ImmunoTherapy of Cancer* 2024;**12**:e009110. doi:10.1136/jitc-2024-009110

► Additional supplemental material is published online only. To view, please visit the journal online (https://doi.org/10.1136/jitc-2024-009110).

YDV and KB are joint senior authors.

Accepted 27 October 2024

For numbered affiliations see end of article.

Correspondence to
Fien Meeus; fien.meeus@vub.be

ABSTRACT

Background Glioblastoma is the most common lethal primary brain tumor, urging evaluation of new treatment options. Chimeric antigen receptor (CAR)-T cells targeting B7 homolog 3 (B7-H3) are promising because of the overexpression of B7-H3 on glioblastoma cells but not on healthy brain tissue. Nanobody-based (nano)CARs are gaining increasing attention as promising alternatives to classical single-chain variable fragment-based (scFv) CARs, because of their single-domain nature and low immunogenicity. Still, B7-H3 nanoCAR-T cells have not been extensively studied in glioblastoma.

Methods B7-H3 nanoCAR- and scFvCAR-T cells were developed and evaluated in human glioblastoma models. NanoCAR-T cells targeting an irrelevant antigen served as control. T cell activation, cytokine secretion and killing capacity were evaluated in vitro using ELISA, live cell imaging and flow cytometry. Antigen-specific killing was assessed by generating B7-H3 knock-out cells using Clustered Regularly Interspaced Short Palindromic Repeats (CRISPR)/Cas9-genome editing. The tumor tracing capacity of the B7-H3 nanobody was first evaluated in vivo using nuclear imaging. Then, the therapeutic potential of the nanoCAR-T cells was evaluated in a xenograft glioblastoma model.

Results We showed that B7-H3 nanoCAR-T cells were most efficient in lysing B7-H3^{pos} glioblastoma cells in vitro. Lack of glioblastoma killing by control nanoCAR-T cells and lack of B7-H3^{neg} glioblastoma killing by B7-H3 nanoCAR-T cells showed antigen-specificity. We showed in vivo tumor targeting capacity of the B7-H3 nanobody—used for the nanoCAR design—in nuclear imaging experiments. Evaluation of the nanoCAR-T cells in vivo showed tumor control in mice treated with B7-H3 nanoCAR-T cells in contrast to progressive disease in mice treated with control nanoCAR-T cells. However, we observed limiting toxicity in mice treated with B7-H3 nanoCAR-T cells and showed that the B7-H3 nanoCAR-T cells are activated even by low levels of mouse B7-H3 expression.

Conclusions B7-H3 nanoCAR-T cells showed promise for glioblastoma therapy following in vitro characterization, but limiting in vivo toxicity was observed. Off-tumor recognition of healthy mouse tissue by the cross-reactive B7-H3 nanoCAR-T cells was identified as a potential cause for this toxicity, warranting caution when using highly sensitive nanoCAR-T cells, recognizing the low-level expression of B7-H3 on healthy tissue.

WHAT IS ALREADY KNOWN ON THIS TOPIC

⇒ B7 homolog 3 (B7-H3) is a promising chimeric antigen receptor (CAR)-T cell target in glioblastoma and other cancer types. B7-H3 single-chain variable fragment-based (scFv)CAR-T cells show limited benefit in clinical trials. B7-H3 nanobody-based CAR (nanoCAR)-T cells were proposed as a more potent variant of scFvCAR-T cells. Still, B7-H3 nanoCAR-T cells have not yet been extensively tested in glioblastoma.

WHAT THIS STUDY ADDS

⇒ This study shows the potential benefit of B7-H3 nanoCAR-T cells in glioblastoma based on straightforward CAR design and potent in vitro functionality. The tumor targeting ability of the nanobody in vivo allows guidance of anti-B7-H3 CAR-T cell therapy using nuclear imaging. In vivo on-target, off-tumor toxicity following B7-H3 nanoCAR-T cell therapy—cross-reactive to mouse B7-H3—highlights the delicate balance between sensitivity and specificity in CAR-T cell therapy for solid tumors.

HOW THIS STUDY MIGHT AFFECT RESEARCH, PRACTICE OR POLICY

⇒ With B7-H3 considered a promising target antigen and increasing B7-H3 CAR-T cell products being developed, caution is warranted regarding off-tumor CAR-T cell activity when using highly sensitive B7-H3 CARs urging profound preclinical investigation in relevant in vivo models, preceding carefully designed clinical studies evaluating safety in humans.

BACKGROUND

Glioblastoma is the most common malignant primary brain tumor, characterized by

an aggressive disease course and poor prognosis, with a median overall survival (OS) of <2 years.[1] Standard-of-care consists of maximal safe resection surgery, followed by combined radiotherapy and temozolomide chemotherapy. However, relapse is inevitable and treatment regimens at this stage are less defined. Resection is often complemented with systemic therapy, like chemotherapy or targeted therapies (eg, bevacizumab). Yet, little evidence exists of any of these treatment regimens prolonging OS, and 5-year survival ultimately remains <10%, leaving a high clinical need for new effective therapies.[1]

While many advances were obtained in immunotherapy for other tumor types, including melanoma and lung cancer, brain tumors were generally marked as ineligible for immunotherapeutic approaches, because of their protection by the blood-brain barrier (BBB).[2 3] The finding that peripheral immune cells can cross the BBB after antigen recognition, and the existence of a brain lymphatic system, invalidated the prevailing idea of the brain as an immune-privileged site, and provided a rationale for the development of immunotherapy for glioblastoma.[4–6] A range of immunotherapeutic approaches is now under investigation, including therapeutic vaccines, oncolytic viruses and immune checkpoint inhibition (ICI). However, besides some isolated reports of responses initial results are disappointing, with many trials unable to show significant efficacy.[1 3 7 8]

In addition to biological factors, like protection by the BBB, disappointing results are mainly attributed to the highly immunosuppressive nature of the glioblastoma tumor microenvironment (TME), leading to T cell exhaustion and tumor immune escape.[4 9] Besides the immunosuppressive TME, to which both tumors as well as immune cells contribute, implementation of immunotherapy regimens for patients with glioblastoma has been difficult due to its characteristic low tumor mutational burden and defects in antigen-processing, leading to the limited presentation of immunogenic antigens. This makes patients with glioblastoma less eligible for immunotherapeutic approaches depending on the presence of neoantigens and endogenous immune responses such as ICI and vaccination.[2] Chimeric antigen receptor (CAR)-T cells represent a promising avenue, as they recognize surface-expressed antigens independent of human leukocyte antigen (HLA)-peptide recognition by the T cell receptor. Here, T cells of a patient are engineered to express so-called “CARs”, in which the antigen-recognition capacity of antibodies is combined with T cell costimulatory and activating domains.[10] In this way, issues such as lack of neoantigens, or altered HLA-peptide presentation are circumvented.

Multiple antigens on glioblastoma cells have been identified that may serve as targets for CAR-T cells. To date, CARs targeting epidermal growth factor receptor variant III, human epidermal growth factor receptor 2 (HER2), ephrin type-A receptor 2 and interleukin (IL)-13 receptor alpha 2 and disialoganglioside GD2 have progressed furthest and entered phase I clinical testing.[2 11–16] While results from these trials show the ability of CAR-T cells to infiltrate the glioblastoma TME and exert antitumor functions, they also show the inability to provide lasting responses and relapse to the therapy is reported in each case.[12 17] Tissue sample analysis revealed decreased levels of antigen-positive cells, installing tumor escape by selection of antigen-negative cells in a heterogeneous tumor.[2 4] Indeed, CAR-T cell therapy has obtained its most promising results in hematological malignancies, presenting with clonal tumor growth and homogenous antigen expression profiles within tumors. This clonality is not common in glioblastoma—and solid tumors in general—where antigen distribution is notoriously heterogeneous. Solutions to this include targeting multiple antigens simultaneously or identification of antigens with more homogenous expression profiles.[18]

B7 homolog 3 (B7-H3, CD276) is a pan-cancer antigen with expression across multiple tumor types, and most importantly with homogenous expression within tumors.[19 20] B7-H3 exists in two isoforms differentiated by a single or double pair of immunoglobulin (Ig) variable and constant domains. The 4 Ig isoform is predominant in humans, while in mice only the 2 Ig isoform occurs. The amino acid sequence has been well-preserved showing an 88% sequence homology between the human and murine variant.[21 22] B7-H3 messenger RNA (mRNA) expression is found in most normal tissues, while protein expression is low and relatively limited, due to post-transcriptional regulation by microRNA.[23 24] In contrast, both B7-H3 mRNA and protein expression on tumor cells of various histological origin and their vasculature is high, with limited heterogeneity.[7 20 21] In the context of glioblastoma, B7-H3 expression is found in more than half of the patients and a negative correlation between tumor mRNA levels and survival has been reported.[7] A case report on a patient with recurrent glioblastoma treated with intracranial B7-H3 CAR-T cell infusions described the initial reduction of the recurrent tumor. Clinical response was sustained for 50 days post CAR-T cell infusion, after which tumor recurrence was observed, highlighting the need for further improvements.[25]

Besides the targeted antigen, shortcomings of CAR-T cell therapy may lie in the CAR design itself.[26] Often, CARs are designed with a single-chain variable fragment (scFv) that is derived from a monoclonal antibody. The scFv consists of a heavy-chain variable fragment (V_H) that is connected to a light-chain variable fragment (V_L) through a peptide linker. However, some drawbacks have been associated with their structure in a CAR context. As scFvs are dimeric proteins and possess hydrophobic interaction regions, self-aggregation on the T cell surface and mispairing of V_H-V_L domains can occur, leading to antigen-independent T cell activation and exhaustion. Moreover, since scFvs are often derived from murine antibodies and possess an artificial peptide linker connecting the V_H to the V_L, they can be immunogenic. In addition, reformatting antibodies towards scFvs may require

extensive linker optimization, to preserve V-region pairing. Nanobodies derived from camelid heavy chain-only antibodies provide an interesting alternative, as the antigen-binding part consists of a single variable domain, the V_HH or nanobody. Their single-domain nature and high sequence homology with human V_H3 genes, render these proteins highly soluble, low immunogenic and easy to engineer, avoiding the occurrence of tonic signaling, the need for linker-sequence optimization or humanization steps.[26 27] In addition to this, using nanobodies in CARs confers the additional opportunity to use the nanobodies as a diagnostic tool, by transforming them into an imaging tracer, to stratify patients before and as follow-up on the nanobody-based CAR (nanoCAR)-T cell therapy.[28] Altogether, these features render nanobodies particularly suited for use in CAR design.[26 28 29] In February 2022, the first nanoCAR-T cell product was approved by the Food and Drug Administration for patients with relapsed and refractory multiple myeloma, paving the way for regulatory approval of these newer constructs for additional indications.

We describe the development and validation of B7-H3 nanoCAR-T cells in glioblastoma. B7-H3 nanoCAR-T cells were evaluated in vitro for activation, cytokine secretion, and antigen-specific killing capacity. NanoCAR-T cells showed strong functionality, evidenced by increased NFAT-signaling, upregulation of 4-1BB, secretion of interferon gamma (IFN-γ), and killing of B7-H3^{pos} but not B7-H3^{neg} glioblastoma cells. In vivo tumor targeting using the radiolabeled B7-H3 nanobody suggested the potential for an image-guided "theranostic" approach. Subsequent evaluation of nanoCAR-T cells in vivo showed tumor growth control by B7-H3 nanoCAR-T cells, which was associated with limiting toxicity, warranting caution when using highly sensitive nanoCARs targeting B7-H3.

Mice, cell lines and primary T cells

Six-week-old athymic Crl:NU(NCr)-Fox1^{nu} or NOD/*SCID*/*IL2Rγ*$^{-/-}$ (NSG) mice (Charles River) were used for imaging or therapy experiments, respectively. Mouse melanoma B16-F10, mouse colorectal cancer CT26, human embryonic kidney 293T, human glioblastoma LN229 and U87, Jurkat-76 cells and their variants used in this study, were cultured as recommended. Peripheral blood mononuclear cells (PBMCs) were isolated from healthy donors after written informed consent using an apheresis device before freezing and storage. Additional details are in (online supplemental methods).

Generation and characterization of lentiviral vectors

An anti-B7-H3 nanoCAR was designed based on a previously described nanobody.[30] A nanoCAR specific for the 5T2 multiple myeloma idiotype (5T2Id) based on the R3B23 nanobody sequence,[31] and a HER2-targeting CAR based on the trastuzumab-derived 4D5 scFv sequence,[32] were generated as controls. The scFv, to produce a B7-H3 scFvCAR, was generated using the variable sequences of enoblituzumab, connected in the orientation of the V_H followed by the V_L using the flexible $(GGGGS)_3$ intrachain linker. Coding sequences were ligated in the pHR' vector to the hinge and transmembrane domain of human CD8α and the cytoplasmic domain of 4-1BB and CD3ζ (figure 1A). The following plasmids were used in this study: pCCL transfer plasmids encoding Katushka2S or eGFP, pLP transfer plasmids encoding NFAT-GFP or Cas9, pLKO transfer plasmid encoding human B7-H3 gRNAs, pHR' transfer plasmids encoding B7-H3 nanoCAR, 5T2Id nanoCAR, B7-H3 scFvCAR, fLuc, or mouse B7-H3. Lentiviral vectors were produced, and functional titers were determined as described.[33 34] Additional details are in online supplemental methods.

Lentiviral modification of human and mouse cells

The following cell lines were generated for this study: GFP^{pos} LN229 and U87 cells, fLuc^{pos} LN229 cells, B7-H3^{KO} Katushka2S^{pos} LN229 cells, mouse B7-H3 overexpressing CT26 cells, B7-H3 nanoCAR^{pos}, B7-H3 scFvCAR^{pos} and 5T2Id nanoCAR^{pos} NFAT-GFP^{pos} Jurkat-76 reporter T cells. Primary CAR-T cells were generated as described,[35] with lentiviral vectors at a multiplicity of infection of 2.5. Cultures were expanded every 2–3 days until harvest at day 10–11, for analysis and use in assays. Additional details are in online supplemental methods.

B7-H3 nanobody and scFv production and characterization using surface plasmon resonance

Production and purification of the B7-H3 scFv, and B7-H3 and 5T2Id nanobodies was performed as described.[36] Affinity parameters of the purified B7-H3 nanobody for recombinant human and mouse B7-H3 protein and for the purified B7-H3 scFv for recombinant human protein were determined by surface plasmon resonance (SPR) on a Biacore T200 instrument (GE Healthcare) determining the equilibrium dissociation constant (K_D). Competition studies for epitope binding of the scFv and nanobody on recombinant human B7-H3 were also determined by SPR on a Biacore T200 instrument (GE Healthcare), as described before.[37] Additional details are in online supplemental methods.

Flow cytometry

Reagents were used according to the manufacturer's instructions or developed protocols. The FcR blocking reagent (Miltenyi Biotec) and fixable viability dye Zombie Aqua (BioLegend) were used when appropriate. Other reagents were: 123count eBeads (Thermo), His_6-tagged nanobodies, biotinylated recombinant B7-H3 antigen (ACROBiosystems), phycoerythrin (PE)-labeled streptavidin (eBioscience), and antibodies against His_6 (PE, Miltenyi Biotec), V_HH (biotinylated, GenScript), Thy1.1 (Alexa Fluor (AF) 647 or PE), 4-1BB (PE), CD25 (BV605), CD69 (PerCP/Cy5.5), human CD45 (AF700), mouse CD45 (APC-Cy7), B7-H3 (PE-Cy7) or isotype-matched controls (PE-Cy7). Antibodies were from BioLegend unless stated otherwise. Expression of GFP and Katushka2S was evaluated without additional staining steps. All samples were

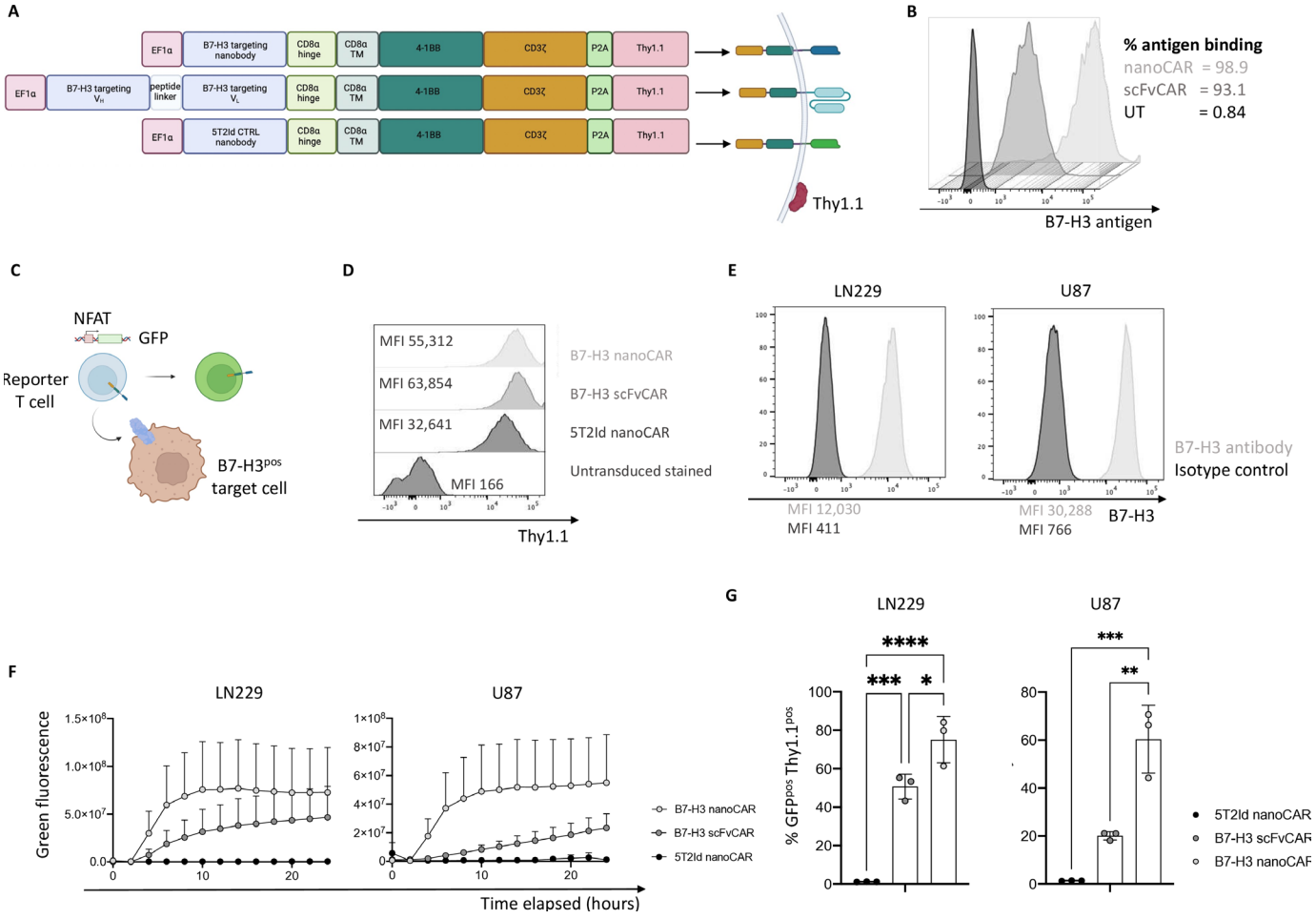

Figure 1 B7-H3 nanoCARs induce strong activation signaling in T cells on recognition of glioblastoma cells. (A) Graphical representation of CAR constructs. (B) Binding capacity of cell-expressed CARs to soluble, recombinant human B7-H3 protein. (C) Graphical representation of a reporter T cell line harboring GFP under control of a NFAT-dependent promoter. (D) CAR expression as determined by Thy1.1 reporter expression on reporter T cells. (E) B7-H3 expression on two glioblastoma cell lines: LN229 and U87. (F) Quantified increase in green fluorescence of Jurkat-76 reporter T cells on co-culture with target cells, as evaluated by IncuCyte live cell imaging. (G) % GFP^{pos} $Thy1.1^{pos}$ cells after 24 hours of co-culture, as determined by flow cytometry. Data represent mean±SD n=3, independent experiments. *p≤0.05; **p≤0.01; ***p≤0.001; ****p≤0.0001. Statistical significance was determined by one-way ANOVA with Tukey's multiple comparisons correction in panel G. 5T2Id, 5T2 multiple myeloma idiotype; ANOVA, analysis of variance; B7-H3, B7 homolog 3; CAR, chimeric antigen receptor; MFI, mean fluorescence intensity; nanoCAR, nanobody-based chimeric antigen receptor; scFvCAR, single-chain variable fragment-based chimeric antigen receptor; UT, untransduced; V_H, heavy-chain variable fragment; V_L, light-chain variable fragment.

acquired on the LSR Fortessa (Becton Dickinson). Data were analyzed using FlowJo software, V.10.0 (Tree Star). Additional details are in online supplemental methods.

Reporter cell line assay for T cell activation

CAR^{pos} Jurkat-76 cells were co-cultured with human U87 or LN229 cells, or mouse B16, CT26, spleen or bone marrow cells at an effector-to-target ratio of 1:1 for 24 hours in the IncuCyte device. The percentage of GFP^{pos} cells in the CAR-T cell fraction ($Thy1.1^{pos}$) was quantified using flow cytometry. Additional details are in online supplemental methods.

Primary CAR-T cell activation assay

CAR-T cells were co-cultured with LN229 cells at an effector-to-target ratio of 1:1 for 24 hours. Secreted cytokines (IFN-γ and IL-2) were measured by ELISA (Thermo), while 4-1BB expression on CAR-T cells was evaluated by flow cytometry. In another experiment, CAR-T cells were co-cultured with spleen or bone marrow cells from NSG mice at an effector-to-target ratio of 1:1 for 24 hours. 4-1BB, CD25 and CD69 expression on CAR-T cells was evaluated by flow cytometry. Additional details are in online supplemental methods.

In vitro and ex vivo CAR-T cell killing assays

CAR-T cells were co-cultured for 48 hours with GFP^{pos} U87 or LN229 cells at an effector-to-target ratio of 2:1 or 1:1, respectively, in the absence of exogenous cytokines. Reduction in green fluorescence was evaluated using IncuCyte (Essen Bio). Target cell killing was quantified using 123count eBeads (Thermo) and flow cytometry. To verify antigen-specific killing, CAR-T cells were

co-cultured for 48 hours with a 1:1 mix of GFP^{pos} B7-H3^{pos} LN229 cells and Katushka2S^{pos} B7-H3^{KO} LN229 cells at an effector-to-target ratio of 2:1 in the absence of exogenous cytokines. Green and red fluorescence were imaged using IncuCyte real-time cell imaging (Essen Bio). The percentage of target-specific killing was quantified as previously described.[38] To assess the killing of spleen and bone marrow cells from NSG mice, CAR-T cells were co-cultured for 24 hours at an effector-to-target ratio of 1:1, in the absence of exogenous cytokines. Target cell killing was quantified in flow cytometry using a mouse CD45 antibody (APC/Cy7, BioLegend) and 123count eBeads (Thermo). Additional details are in online supplemental methods.

In vivo Single Photon Emission Computed Tomography (SPECT)/CT imaging and ex vivo biodistribution analysis of radiolabeled nanobodies

Mice, subcutaneously inoculated with B7-H3^{pos} U87 cells were followed until tumors reached adequate size for imaging. His_6-tagged nanobodies were site-specifically labeled with Technetium-99m (^{99m}T) as described.[39] Imaging and ex vivo biodistribution analysis was performed as described.[40] Data were normalized to organ weight and corrected for radioactive decay. Additional details are in online supplemental methods.

In vivo xenograft model

Mice were injected subcutaneously in the right flank with 1×10^6 B7-H3^{pos} fLuc^{pos} LN229 cells. Three days later, mice were injected intraperitoneally (i.p.) with D-luciferin (Promega) for bioluminescence imaging in an IVIS device. One day later, 5×10^6 CAR-T cells were injected intravenously. Blood was collected on weeks 1 and 3 after adoptive cell transfer. Tumor growth was evaluated three times per week until humane endpoints were reached. In another experiment, mice were left without tumors and injected intravenously with 5×10^6 CAR-T cells. Blood was collected on weeks 3, 4 and 5 after adoptive cell transfer at which point mice were sacrificed. Hematological analysis of blood at week 5 was performed using the scil Vet abc Plus. Additional details are in online supplemental methods.

Immunohistochemistry

To assess CAR-T infiltration, murine organs and tissues such as the brain, heart, lungs, liver, spleen, kidney and small intestine were fixed in 4% paraformaldehyde for 24 hours at 4°C, transferred to 70% ethanol at 4°C and paraffin-embedded. Femurs were fixed in 4% paraformaldehyde for 24 hours at 4°C, transferred to 0.45M EDTA for 72 hours at 4°C on a shaker, transferred to 70% ethanol and paraffin-embedded. Blocks were sectioned at 4µm, mounted onto Superfrost Plus slides (VWR, Heverlee, Belgium) and dried overnight at 42°C. Sectioning, staining and scanning were performed by the Visual and Spatial Tissue Analysis core facility at Vrije Universiteit Brussel (https://vsta.research.vub.be). Additional details on antigen retrieval and staining of human CD3 are in online supplemental methods.

Statistical analysis

Statistical analyses were performed with GraphPad Prism V.9 software. Data are represented as mean±SD. Biological replicates represent individual donors or mice. The replicate number is provided in the figure legends. Statistical significance was determined using unpaired t-tests, one or two-way ANOVA followed by Welch's, Tukey's, Dunnett's or Bonferroni's post hoc test for multiple comparison correction. P values were reported as follows: *p≤0.05; **p≤0.01; ***p≤0.001; ****p≤0.0001.

RESULTS

B7-H3 nanoCARs induce strong activation signaling in T cells on recognition of B7-H3^{pos} glioblastoma cells

The coding sequence of a B7-H3 nanobody[30] was used to generate a nanoCAR in which the nanobody is followed by the CD8α hinge and transmembrane domains, and intracellular 4-1BB and CD3ζ signaling domains. The CAR sequence is followed by the P2A and Thy1.1 sequence allowing Thy1.1 expression on the cell surface for evaluation of transduction efficiency. As a benchmark, we generated a scFvCAR incorporating the V_H and V_L domains of enoblituzumab. The 5T2 mouse myeloma idiotype (5T2Id)-specific nanoCAR was generated as a control. The design of the constructs is shown in figure 1A. Retention of B7-H3 antigen-binding ability on expression as CARs on T cells was confirmed by a flow cytometry-based binding assay for the scFvCAR and nanoCAR (figure 1B). Correlation of CAR and Thy1.1 expression was confirmed using flow cytometry, justifying the use of the Thy1.1-reporter as a proxy for CAR expression (online supplemental figure 1A).

To evaluate the ability of the CARs to induce T cell activation on antigen encounter, we generated a Jurkat-76 reporter T cell line in which GFP expression is driven by a NFAT-dependent promotor, signifying CAR/CD3ζ signaling (figure 1C). CAR^{pos} Jurkat-76 reporter cells were generated through lentiviral transduction. Expression of the CAR constructs on cells was validated using flow cytometry (figure 1D). B7-H3 expression on glioblastoma LN229 and U87 cells was confirmed using flow cytometry (figure 1E). Ability of the CAR constructs to induce T cell activation was evaluated by co-culturing the CAR^{pos} Jurkat-76 reporter cells with glioblastoma target cells. The increase in GFP signal over time was quantified using live cell imaging (figure 1F). Images at 18 hours post co-culture are shown in online supplemental figure 1B. Moreover, flow cytometric analysis following co-incubation with both cell lines showed GFP expression in B7-H3 nanoCAR^{pos} and scFvCAR^{pos} Jurkat-76 reporter cells (figure 1G). The B7-H3 nanoCAR was most effective in activating NFAT-signaling, while no NFAT-signaling was observed in the Jurkat-76 reporter cells expressing the 5T2Id nanoCARs (figure 1G). This was confirmed using

separate transductions of Jurkat-76 cells, as summarized in online supplemental figure 1C–H . Despite similar expression levels of B7-H3 on LN229 and U87 cells, nano and scFvCARs were more potently activated against LN229 cells (figure 1G).

B7-H3 nanoCAR-T cells kill B7-H3^{pos} glioblastoma cells in vitro in an antigen-specific manner

On confirming the functionality of the CARs in the reporter T cell assay, cytotoxicity of CAR-transduced primary T cells against B7-H3^{pos} glioblastoma cells was evaluated (figure 2A). Transduction efficiency for all constructs was over 95% (figure 2B). To evaluate killing of glioblastoma cells by the different CAR-T cells, we generated GFP^{pos} LN229 cells (figure 2C). Following

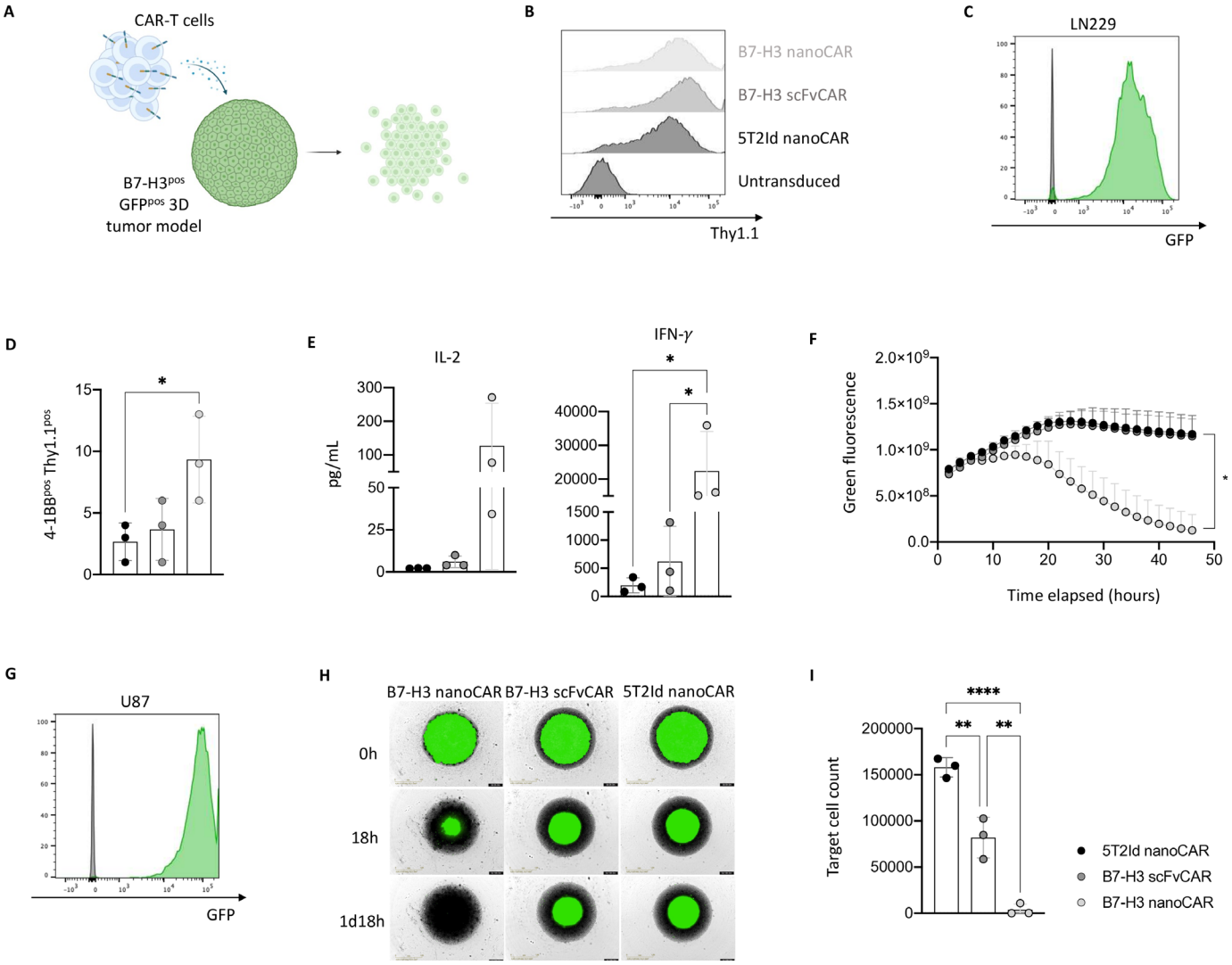

Figure 2 B7-H3 nanoCAR-T cells kill glioblastoma cells in vitro and secrete high levels of IFN-γ. (A) Graphical representation of CAR-T cell mediated cell killing of GFP^{pos} B7-H3^{pos} three-dimensional tumor models. (B) CAR transduction efficiency of expanded primary T cells based on Thy1.1 expression at day 10 post-transduction. (C) GFP expression in LN229 cells stably transduced with GFP-encoding lentiviral vectors. (D) 4-1BB expression on CAR-T cells on co-culturing with LN229 cells. (E) IL-2 and IFN-γ levels secreted by CAR-T cells on co-culturing with LN229 cells. (F) Quantified live cell imaging from IncuCyte showing killing of GFP^{pos} three-dimensional LN229 tumor models by CAR-T cells. (G) GFP expression in U87 cells stably transduced with GFP-encoding lentiviral vectors. (H) Live cell images from IncuCyte showing killing of GFP^{pos} three-dimensional U87 tumor models by CAR-T cells, as shown for one representative donor. (I) End-point flow cytometric analysis of absolute target cell counts after co-culturing with CAR-T cells. Data represent mean±SD n=3, biological repeats. Each dot represents a different donor. * p≤0.05; **p≤0.01; ****p≤0.0001. Statistical significance was determined by one-way ANOVA with Tukey's multiple comparisons correction in panel D, E and I. Two-way ANOVA with Dunnett's multiple comparisons test was used to determine statistical significance in panel F (significance shown on the graph for the last time point (48 hours), comparing the B7-H3 and 5T2Id nanoCAR conditions). 5T2Id, 5T2 multiple myeloma idiotype; ANOVA, analysis of variance; B7-H3, B7 homolog 3; CAR, chimeric antigen receptor; IFN-γ, interferon gamma; IL-2, interleukin-2; nanoCAR, nanobody-based chimeric antigen receptor; scFvCAR, single-chain variable fragment-based chimeric antigen receptor.

coincubation of CAR-T and LN229 cells, upregulation of the activation marker 4-1BB was evaluated as a first sign of CAR-T functionality, showing the highest upregulation of 4-1BB in B7-H3 nanoCAR-T cells (figure 2D). Evaluation of cytokine secretion in the supernatants on co-culturing with target cells revealed production of IL-2 and IFN-γ, with the highest levels of IFN-γ being produced by the B7-H3 nanoCAR-T cells (figure 2E). B7-H3 scFv-CAR-T cells showed lower levels of IFN-γ production, suggesting a lower functionality. The killing of the LN229 glioblastoma target cells by the different CAR-T cells was evaluated using an in vitro three-dimensional killing assay. Live cell imaging showed complete eradication of three-dimensional LN229 tumor models by the B7-H3 nanoCAR-T cells but not scFvCAR-T cells (online supplemental figure 2A), as quantified in figure 2F. To extend these data, GFP^{pos} U87 glioblastoma target cells were generated (figure 2G). Live cell images showed complete eradication of three-dimensional U87 tumor models by the B7-H3 nanoCAR-T cells but not scFvCAR-T cells (figure 2H). Flow cytometric analysis of target cell counts after co-culture confirmed image analysis, showing complete rejection of target cells when cultured with B7-H3 nanoCAR-T cells, but only partial rejection by B7-H3 scFvCAR-T cells as compared with the co-culture with 5T2Id nanoCAR-T cells (figure 2I).

To evaluate whether the effective killing of B7-H3^{pos} glioblastoma cells by the nanoCAR-T cells is target-specific, we used an antigen-specific three-dimensional killing assay (figure 3A). To this end, we generated B7-H3 knock-out LN229 glioblastoma cells, using CRISPR/Cas9 genome editing (figure 3B). Then, we generated GFP^{pos} target and Katushka2S^{pos} non-target variants of the wild type and B7-H3^{KO} LN229 cells, respectively (figure 3C).

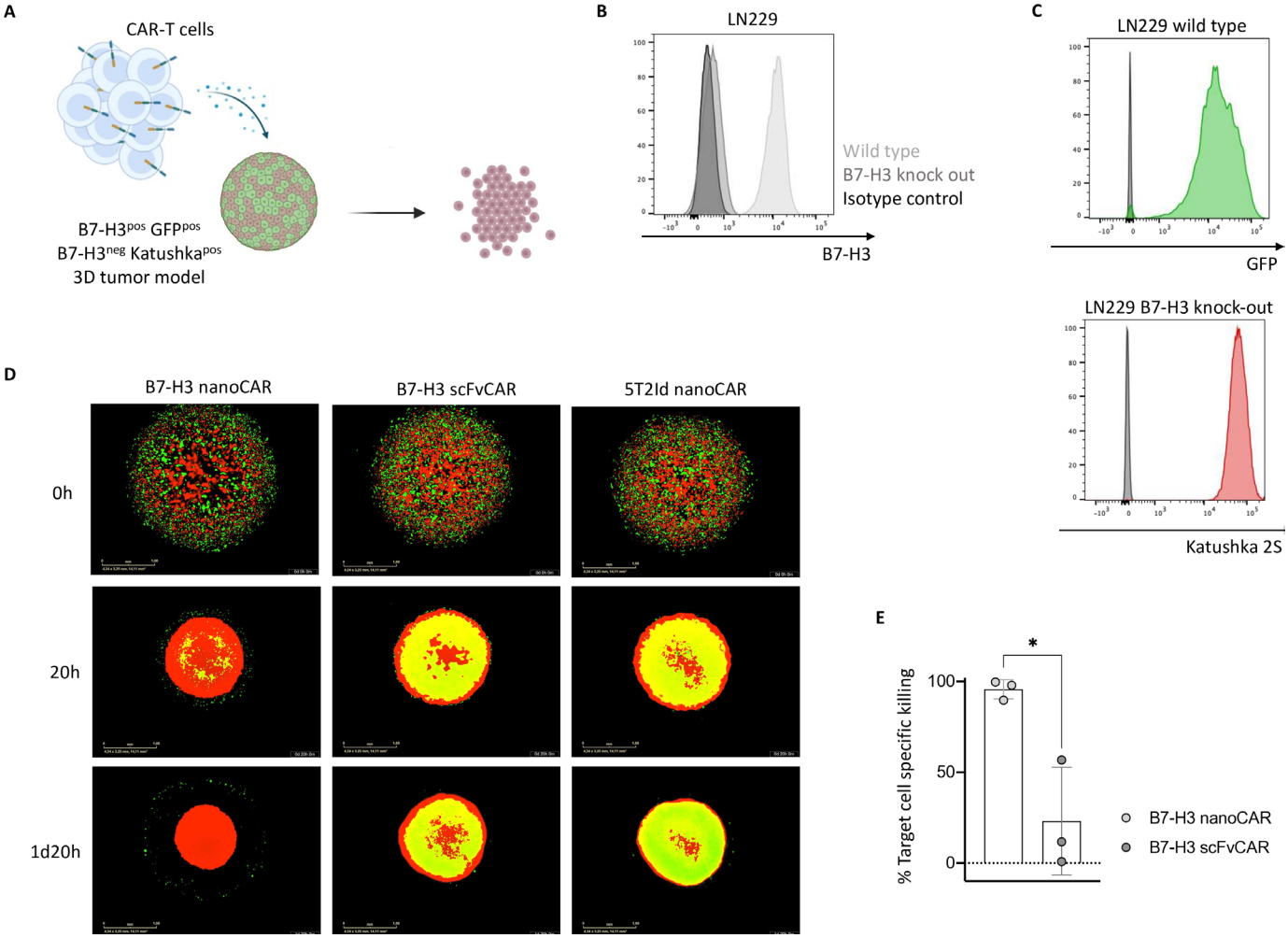

Figure 3 Killing by B7-H3 nanoCAR-T cells is antigen-specific. (A) Graphical representation of CAR-T cell killing of GFP^{pos} B7-H3^{pos} LN229 glioblastoma cells but not Katushka2S^{pos} B7-H3^{neg} LN229 cells. (B) B7-H3 expression on wild type LN229 cells and B7-H3 knock-out LN229 cells. (C) GFP expression in wild type LN229 cells and Katushka2S expression in B7-H3 knock-out LN229 cells, following stable transduction with lentiviral vectors. (D) Live cell images from IncuCyte showing killing of GFP^{pos} target cells but not Katushka2S^{pos} non-target cells in three-dimensional tumor models by CAR-T cells, as shown for one representative donor. (E) End-point flow cytometric analysis of % target cell specific killing. Data represent mean±SD n=3, biological repeats. Each dot represents a different donor. *p≤0.05. Statistical significance in panel E was determined using an unpaired t-test. 5T2Id, 5T2 multiple myeloma idiotype; B7-H3, B7 homolog 3; CAR, chimeric antigen receptor; nanoCAR, nanobody-based chimeric antigen receptor; scFvCAR, single-chain variable fragment-based chimeric antigen receptor.

Equal amounts of target and non-target cells were grown in three-dimensional models before adding the different CAR-T cells. Live cell imaging showed complete rejection of GFP^{pos} target cells in co-cultures with B7-H3 nanoCAR-T cells, while no clear difference between the co-cultures with B7-H3 scFvCAR-T cells and 5T2Id nanoCAR-T cells could be observed (figure 3D). Flow cytometry analysis of the cultures allowed to determine the percentage of target cell-specific killing, as compared with the 5T2Id nanoCAR-T cell control. NanoCAR-T cells specific for B7-H3 showed approximately 100% target cell-specific killing, in contrast to B7-H3 scFvCAR-T cells that showed a weaker killing efficiency (figure 3E).

B7-H3 nanobodies have potent in vivo tumor-targeting capacity

To understand the difference in potency between nanoCAR and scFvCAR-T cells, we assessed the characteristics of their targeting moieties as soluble proteins. Affinity (K_D) for the human B7-H3 antigen was determined using SPR, revealing nanomolar affinities of 14.5 nM and 60 nM for the nanobody and scFv, respectively (figure 4A and B). Using a competition study for binding to B7-H3 protein, we observed that both targeting moieties bind two different epitopes on B7-H3 (figure 4C). Given these differences and because of the superior activity of the nanobody in our CAR, we excluded the scFvCAR for further in vivo evaluation.

Nanobodies possess advantageous features for use as imaging tracers. Therefore, in vivo tumor targeting capacity of the nanobody used to design the B7-H3 nanoCAR was evaluated to assess the imaging potential of this nanobody. This would allow identifying patients who are eligible for B7-H3 CAR-T cell therapy. To evaluate the nanobody's in vivo tumor tracing capacity of transplanted

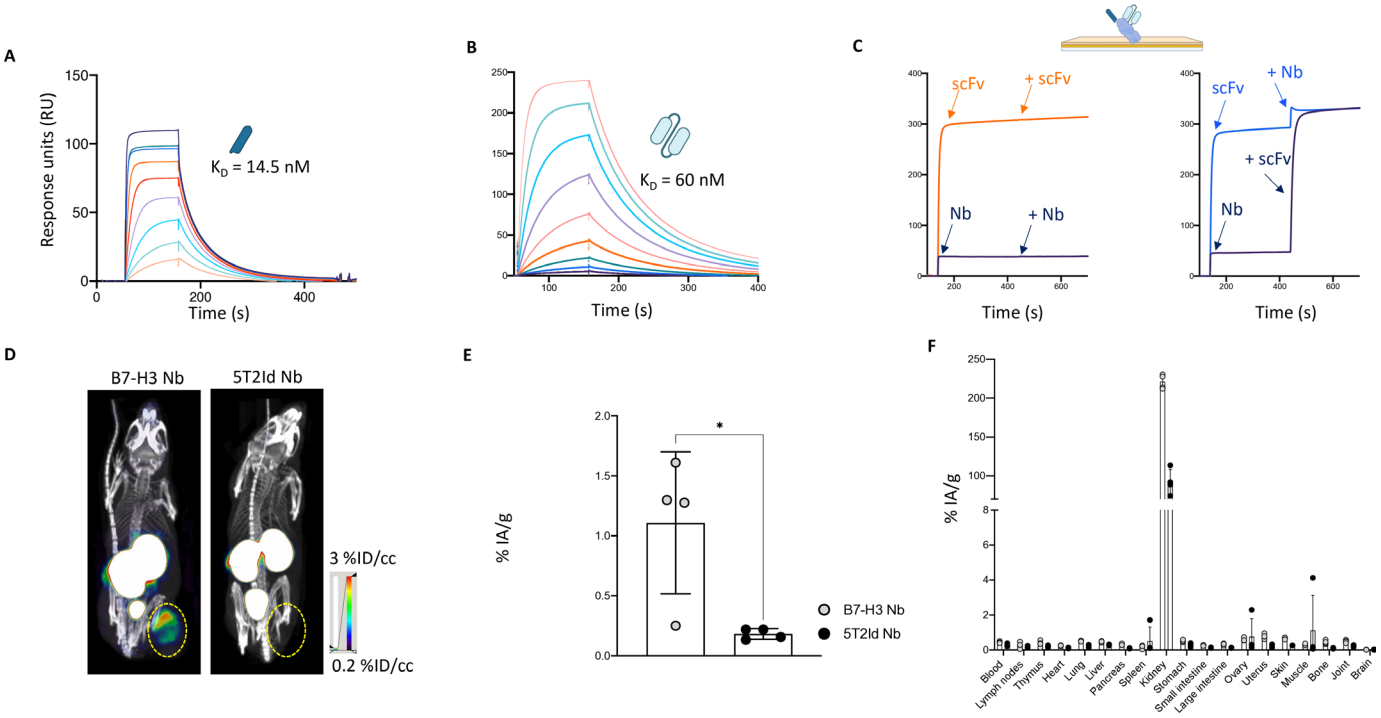

Figure 4 Radiolabeled B7-H3 nanobody has potent in vivo tumor targeting capacity. (A) Evaluation of binding kinetics of purified B7-H3 nanobody on immobilized recombinant human B7-H3 protein using SPR. The sensorgram represents binding and dissociation of a dilution series (1/2 dilution series ranging from 500 nM to 3.9 nM) of the nanobody. Binding kinetics were calculated using the Biacore T200 V.2.0 evaluation software to calculate the K_D value. (B) Evaluation of binding kinetics of purified B7-H3 scFv on immobilized recombinant human B7-H3 protein using SPR. The sensorgram represents binding and dissociation of a dilution series (1/2 dilution series ranging from 500 nM to 1.9 nM) of the scFv. Binding kinetics were calculated using the Biacore T200 V.2.0 evaluation software to calculate the K_D value. (C) Competition study of the B7-H3 nanobody and scFv showing that both bind a different epitope on human B7-H3, as determined by SPR. The absence of competition is shown by the increase in signal obtained by binding of the competitor in a second association step (right panel) as compared with the signal obtained by the individual components (left panel). (D) Representative SPECT/CT images of tumor-bearing mice 1 hour postinjection with radiolabeled B7-H3 or 5T2Id nanobodies. The images are representative for three mice. Yellow circles indicate tumor positioning. (E) Graph of percentages injected activity per gram (%IA/g) for isolated tumors as determined by ex vivo γ-counting. The graph summarizes the tumor uptake of the B7-H3 and 5T2Id nanobody in four mice. (F) Graph of percentages injected activity per gram (%IA/g) for all isolated organs and tissues as determined by ex vivo γ-counting. The graph summarizes the biodistribution of the B7-H3 and 5T2Id nanobody in four mice. Data represent mean±SD n=4 mice per group. *p≤0.05. Statistical significance in panel E was determined using an unpaired t-test. 5T2Id, 5T2 multiple myeloma idiotype; B7-H3, B7 homolog 3; K_D, equilibrium dissociation constant; Nb, nanobody; scFv, single-chain variable fragment; SPECT, single photon emission computed tomography; SPR, surface plasmon resonance.

B7-H3^{pos} human glioblastoma cells, B7-H3 or 5T2Id nanobodies were radiolabeled with ^{99m}Tc. Immunedeficient mice that were subcutaneously inoculated with U87 cells in their right flank, were injected intravenously with 100 µL ^{99m}Tc-labeled nanobody. SPECT/CT imaging was performed at 1 hour postinjection, after which ex vivo biodistribution was analyzed based on γ-counting of dissected tissues determining tracer uptake. SPECT/CT images show specific uptake of the radiolabeled B7-H3 nanobody at the tumor site, and lack of uptake of the 5T2Id nanobody (figure 4D). High accumulation of radiolabeled nanobodies is observed in the kidneys and bladder, which is expected as nanobodies undergo renal clearance. Data from ex vivo biodistribution analyses confirm the images, showing a significantly higher uptake of the B7-H3 nanobody than 5T2Id nanobody in tumor tissue (figure 4E). Off-tumor uptake in organs other than kidneys is low (figure 4F).

B7-H3 nanoCAR-T cells control tumor growth in vivo but are associated with toxicity events

Next, we evaluated the ability of the B7-H3 nanoCAR-T cells to exert antitumor function in vivo (figure 5A). This was assessed in a murine xenograft model in which NSG mice were subcutaneously injected with fLuc^{pos} LN229 glioblastoma cells. B7-H3 nanoCARs were compared with 5T2Id non-targeting control CARs and HER2-targeting CARs serving as positive control. Tumor engraftment in all mice was confirmed 3 days later using bioluminescence imaging (figure 5B). One day later, adoptive transfer of 5×10^6 CAR-T cells was performed by intravenous injection. T cells modified to express B7-H3, 5T2Id and HER2 CARs showed similar transduction levels of more than 95% before injection (figure 5C). Tumors grew progressively in 5T2Id nanoCAR-T cell treated control mice, while B7-H3 and HER2 CAR-T cells were able to control or completely eradicate tumor growth, respectively, during 24 days following treatment, after which monitoring was stopped (figure 5D). Blood data from weeks 1 and 3 postinfusion revealed strong expansion of CAR^{pos} huCD45^{pos} cells in the circulation of B7-H3 nanoCAR-T cell treated mice (figure 5E). A progressive weight loss in B7-H3 nanoCAR-T cell treated mice was observed, suggesting a B7-H3 nanoCAR-T cell therapy-related toxicity (figure 5F). Because of this B7-H3 nanoCAR-mediated toxicity, mice were sacrificed 24 days after treatment. On dissection of mice, lobular spleens with yellow areas were found (figure 5G). Moreover, the pale color of highly vascularized organs such as the heart, liver and kidneys (online supplemental figure 3B) in B7-H3 nanoCAR-T cell treated mice suggested the development of anemia, which was in line with a decreased visibility of ear veins (online supplemental figure 3A). Since no toxicity occurred in the HER2 CAR-T cell treated group, we excluded graft-versus-host disease (GVHD) as a cause for this toxicity. Instead, we hypothesized that on-target activation against off-tumor tissue might explain the relatively limited antitumor function and the observed toxicity associated with the B7-H3 nanoCAR-T cells.

In vivo toxicity of B7-H3 nanoCAR-T cells may be explained by cross-reactivity to mouse B7-H3 and sensitivity to low levels of endogenous B7-H3 expression on mouse cells

To identify the cause for this B7-H3 nanoCAR-mediated toxicity, we evaluated the possibility of on-target, off-tumor toxicity, since sequence homology between human and mouse B7-H3 reaches 88%.[22] SPR of the nanobody on mouse B7-H3 protein revealed an affinity of 10 nM, indicating that nanobody binding to mouse B7-H3 is in the same affinity range as to human B7-H3, which was 14.5 nM (figure 6A). To evaluate whether the nanobody could also recognize native expression of B7-H3 on mouse cells, we evaluated nanobody binding to mouse melanoma B16 cells, which were reported to express B7-H3.[41] Flow cytometry showed binding of the nanobody to B16 cells, although at low levels (figure 6B). To extend these data, mouse colorectal cancer CT26 cells were also evaluated for binding by the B7-H3 nanobody, showing similar results as for B16 cells (figure 6B). To evaluate whether the relatively weak binding of the B7-H3 nanobody to mouse cells was because of low B7-H3 expression or weaker binding affinity of the nanobody to mouse B7-H3, we generated lentiviral vectors encoding mouse B7-H3 to generate a B7-H3 overexpressing CT26 variant. Staining of mouse B7-H3 overexpressing cells showed 100% nanobody binding, indicating that the nanobody binds well to cell-expressed mouse B7-H3 (figure 6C). To evaluate whether the nanobody, when expressed in a CAR, is able to induce T cell activation on recognition of low levels of mouse B7-H3 expression, we co-cultured the previously generated CAR^{pos} Jurkat-76 reporter T cells with the wild type B16 and CT26 mouse cells. B7-H3 nanoCARs induced GFP expression in reporter T cells on co-culture, while B7-H3 scFvCARs and 5T2Id nanoCARs did not (figure 6D). This indicates that the B7-H3 nanoCAR-T cells are capable of recognizing low-level expression of endogenous mouse B7-H3 and induce CAR signaling and T cell activation on encounter with these cells. NFAT-GFP-signaling was not observed when any of the Jurkat-76 reporter T cells were cultured in the absence of target cells (online supplemental figure 4A).

To link the in vivo B7-H3 nanoCAR-T cell toxicity to the recognition of endogenous mouse B7-H3 on off-tumor tissue, we harvested the spleen and bone marrow of mice, to evaluate whether targeting these hematopoietic organs might cause the observed toxicity (figure 6E). Flow cytometric analysis of nanobody binding on these tissues did not show detectable mouse B7-H3 expression (online supplemental figure 4B). Still, ex vivo co-culturing of these mouse cells with B7-H3 nanoCAR reporter T cells showed the nanoCARs ability to induce CAR signaling and T cell activation, based on NFAT-driven GFP expression, on encounter with these cells, as shown by IncuCyte images (figure 6F) and quantified (online supplemental figure 4C). Moreover, on co-culturing of primary CAR-T

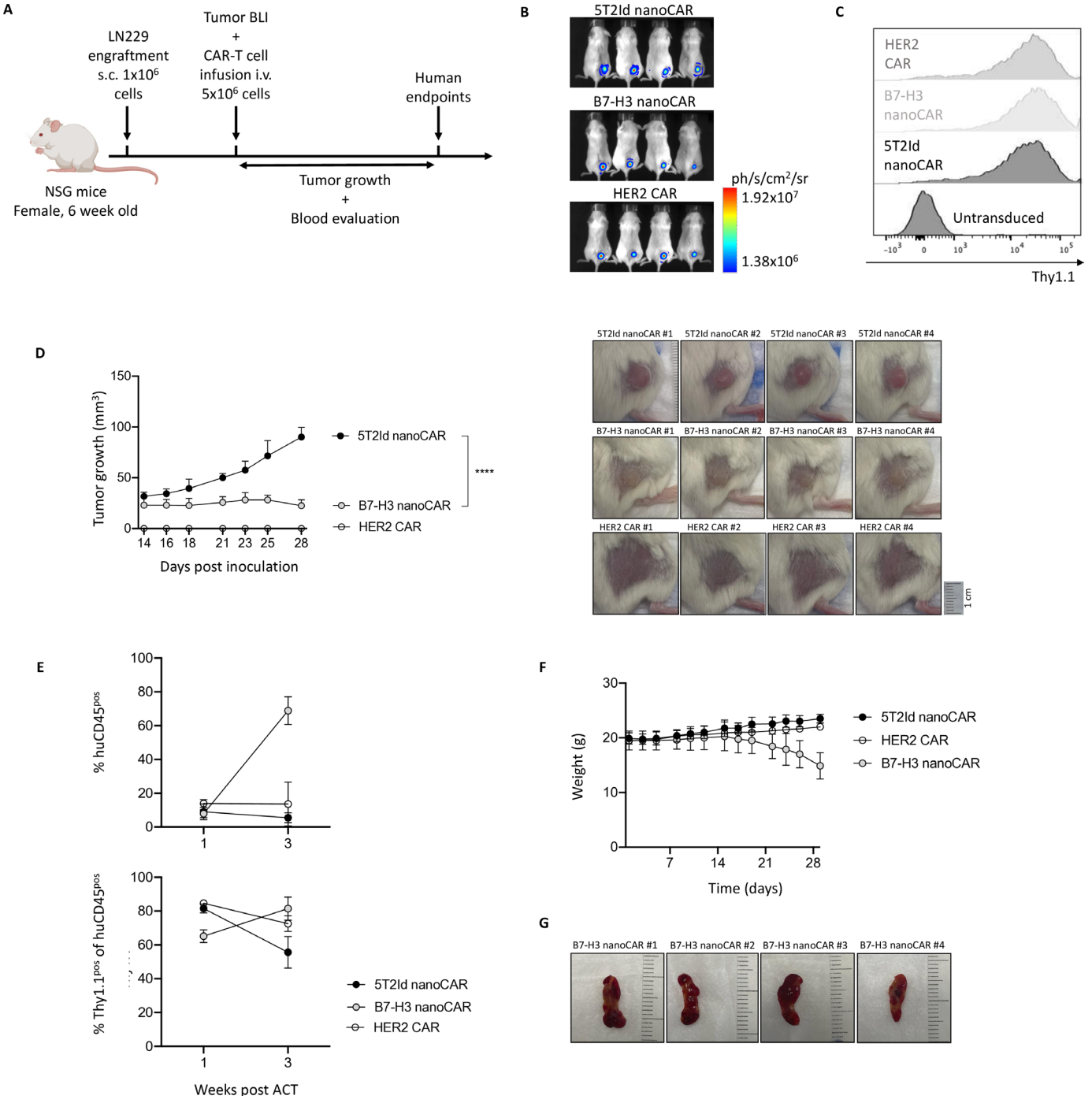

Figure 5 B7-H3 nanoCAR-T cells control tumor growth in vivo but are associated with toxicity events. (A) Graphical overview of in vivo experimental set-up. (B) Bioluminescent images at day 3 post inoculation. (C) Thy1.1 expression of expanded CAR-T cell products at day 10 post-transduction. (D) Tumor growth curves over time (left) and tumor images at 28 days post inoculation, shown for all conditions (right). (E) Flow cytometry data of blood from mice, processed at 1 and 3 weeks of CAR-T cell treatment, showing % of circulating human CD45 cells gated within all living blood cells and Thy1.1 positive cells within the human CD45^{pos} cell population. (F) Weight curves over time. (G) Images of spleens dissected from B7-H3 nanoCAR-treated mice. Data represent mean±SD n=4 mice per group. ****p≤0.0001. Two-way ANOVA with Bonferroni's multiple comparisons test was used to determine statistical significance in panel D. Statistical significance shown on the graph at 28 days post inoculation. 5T2Id, 5T2 multiple myeloma idiotype; ACT, adoptive cell transfer; ANOVA, analysis of variance; B7-H3, B7 homolog 3; BLI, bioluminescence imaging; CAR, chimeric antigen receptor; HER2, human epidermal growth factor receptor 2; i.v., intravenously; nanoCAR, nanobody-based chimeric antigen receptor; s.c., subcutaneously.

cells from three different donors, we observed a slight decrease in target cell counts of moCD45^{pos} cells in the cultures of spleen and bone marrow cells (figure 6G). This was associated with a modest increase in activation markers 4-1BB, CD25 and CD69 in the B7-H3 nanoCAR conditions (figure 6H). Based on these results, we

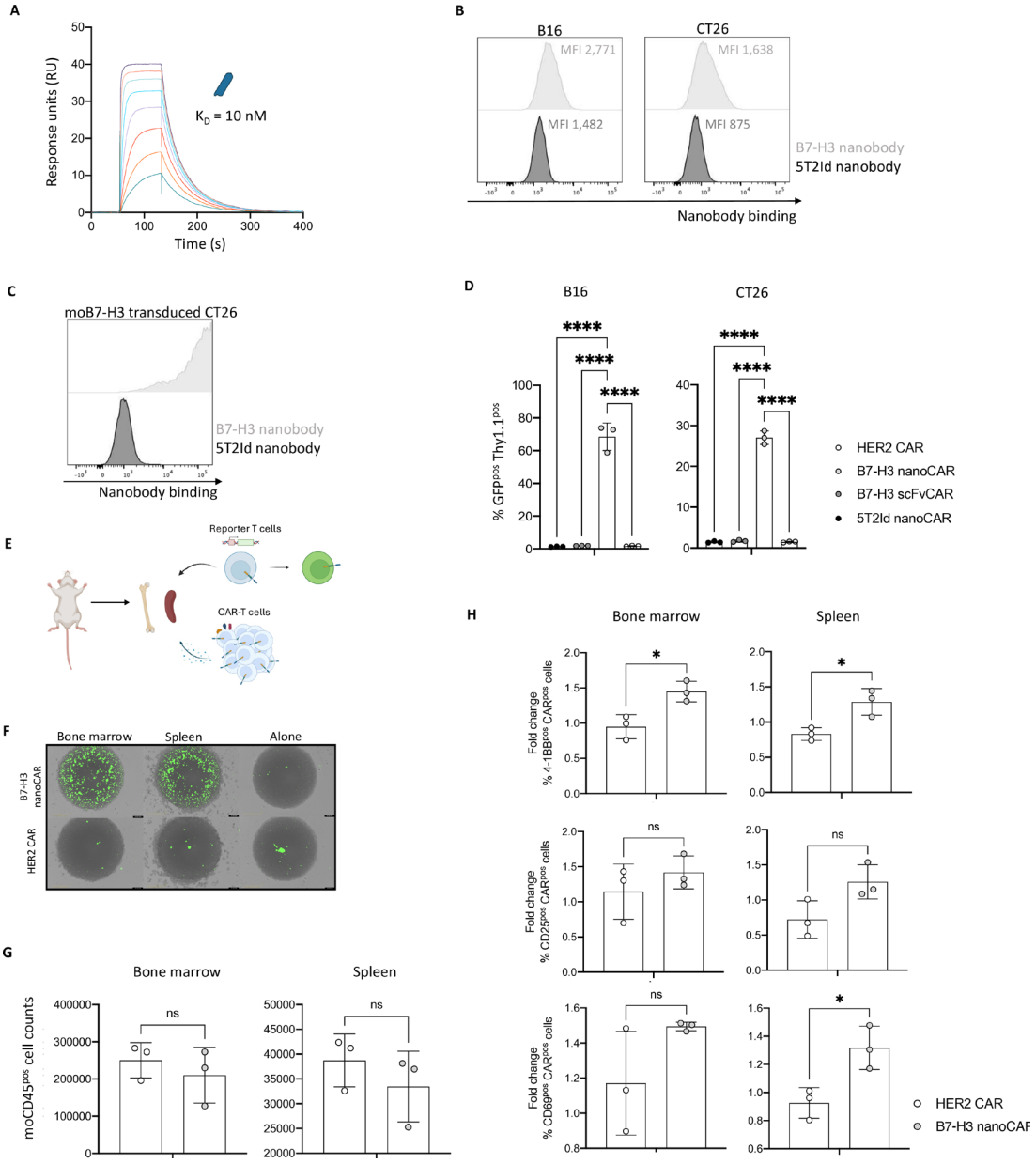

Figure 6 In vivo toxicity of B7-H3 nanoCAR-T cells may be explained by cross-reactivity to mouse B7-H3 and sensitivity to low levels of endogenous B7-H3 expression on mouse cells. (A) Evaluation of binding kinetics of purified B7-H3 nanobody on immobilized recombinant mouse B7-H3 protein using SPR. The sensorgram represents binding and dissociation of a dilution series (1/2 dilution series ranging from 500 nM to 3.9 nM) of the nanobody. Binding kinetics were calculated using the Biacore T200 V.2.0 evaluation software to calculate the K_D value. (B) B7-H3 and 5T2Id nanobody-binding to wild-type B16 and CT26 mouse cells, as determined by flow cytometry. (C) B7-H3 and 5T2Id nanobody-binding to the CT26 mouse cells overexpressing mouse B7-H3 through lentiviral transduction, as determined by flow cytometry. (D) % GFP^{pos} $Thy1.1^{pos}$ cells after co-culture of CAR^{pos} Jurkat-76 reporter T cells with wild type B16 or CT26 mouse cells, as determined by flow cytometry. (E) Graphical overview of ex vivo experimental set-up. (F) Images from IncuCyte live cell imaging after 24 hours of co-culture showing GFP expression in reporter T cells on co-culturing with spleen cells, bone marrow cells, or in the absence of target cells. (G) End-point flow cytometric analysis of absolute target cell counts after co-culturing with CAR-T cells. (H) 4-1BB, CD25 and CD69 expression on CAR-T cells on co-culturing with spleen or bone marrow cells from NSG mice. Data are shown as fold change in activation marker expression of CAR-T cells cultured with target cells relative to the CAR-T cells without target cells, for each separate donor. Data represent mean±SD n=3, independent experiments, in panel D. n=3, biological repeats (from three different donors, and cells pooled from three different mice), in panel G and H. Each dot represents a different donor in panel G and H. *p≤0.05; ****p≤0.0001. Statistical significance was determined by one-way ANOVA with Tukey's multiple comparisons correction in panel D. Statistical significance was determined by unpaired t-tests with Welch's correction in panel G and H. 5T2Id, 5T2 multiple myeloma idiotype; ANOVA, analysis of variance; B7-H3, B7 homolog 3; CAR, chimeric antigen receptor; HER2, human epidermal growth factor receptor 2; K_D, equilibrium dissociation constant; MFI, mean fluorescence intensity; nanoCAR, nanobody-based chimeric antigen receptor; scFvCAR, single-chain variable fragment-based chimeric antigen receptor; SPR, surface plasmon resonance.

hypothesize that the B7-H3 nanoCAR is highly sensitive and capable of inducing CAR signaling on recognition of mouse B7-H3 expression levels that are below the detection limit for flow cytometry, linking the toxicity observed in the in vivo model to reactivity against low endogenous expression of mouse B7-H3 on healthy tissue.

To substantiate whether the observed toxicity occurred as a consequence of on-target, off-tumor toxicity, we evaluated whether B7-H3 nanoCAR-T cells would show reactivity to B7-H3 on healthy mouse tissue in the absence of tumors. To this end, non-tumor-bearing mice were injected with 5×10^6 B7-H3 nanoCAR-T or HER2 CAR-T cells (figure 7A). Blood data from weeks 3, 4 and 5 postinfusion revealed an expansion of huCD45^{pos} cells in the circulation of B7-H3 nanoCAR-T cell-treated mice compared with control mice injected with HER2 CAR-T cells (figure 7B), suggesting an antigen-induced expansion of the B7-H3 nanoCAR-T cells in these mice. Associated with this, two out of three B7-H3 nanoCAR-treated mice showed progressive weight loss (figure 7C). Therefore, mice were sacrificed at week-5 post-CAR-T cell therapy. One mouse (#2) from the B7-H3 nanoCAR-treated group—suffering from the most severe weight loss—showed signs of anemia reminiscent of the anemic appearance of mice in the previous experiment. This was confirmed by hematologic blood analysis showing severe loss of red blood cell, hemoglobin and hematocrit levels in this mouse (#2) (figure 7D). On dissection, spleens from B7-H3 nanoCAR-treated mice again appeared with yellow and lobular regions (figure 7E). Flow cytometric analysis of spleens revealed huCD45^{pos} cell infiltration in spleens from both HER2 CAR and B7-H3 nanoCAR-T cell groups, and a notable decrease in the moCD45^{pos} cell population that was specific to the B7-H3 nanoCAR-T cell group (figure 7F). This was confirmed through immunohistochemical analysis of spleens in which staining for human (hu)CD3 was used to evaluate CAR-T cell infiltration. This showed that CAR-T infiltration in spleens of B7-H3 nanoCAR-T cell treated mice coincided with necrotic regions with loss of hematoxylin-stained cells as a proxy for huCD3^{neg} mouse cells (figure 7G). Looking into the cellular composition of the bone marrow, infiltration of huCD45^{pos} cells was higher in the B7-H3 nanoCAR-T cell group (figure 7H). As we were unable to collect sufficient bone marrow cells from the B7-H3 nanoCAR-T cell treated mouse (#2) presenting with the most severe signs of toxicity (anemia, weight loss) for flow cytometric analysis, femurs were also subject to immunohistochemical analysis. This allowed us to link the development of anemia in B7-H3 nanoCAR mouse #2 to an apparent loss of huCD3^{neg} mouse cells shown by a reduced hematoxylin staining in the femur of this mouse (figure 7I and B–H3 nanoCAR #2), as compared with the HER2 CAR-treated mice (figure 7I, below). Moreover, in line with flow cytometry data, increased infiltration of human T cells in the bone marrow of B7-H3 nanoCAR-T cell treated mice #1 and #3 was observed (figure 7I). Assessing CAR-T cell infiltration in other organs showed patterns expected for xenograft models of CAR-T cell therapy, without notable differences across HER2 CAR- and B7-H3 nanoCAR-T cell groups (figure 7J). Basic phenotype data of CAR-T cell products before and after infusion are provided in online supplemental figure 5.

DISCUSSION

In this study, we designed and validated B7-H3 nanoCAR- and scFvCAR-T cells in the context of glioblastoma in vitro, in terms of activation, cytokine secretion, killing efficiency and antigen-specificity, demonstrating strong functionality of the nanoCAR-T cells but not scFvCAR-T cells in this study. Differences in binding characteristics such as affinity and epitope location between the scFv and nanobody may account for this observation. Moreover, it is possible that the B7-H3 scFvCAR designed for this study did not reach its full potential and could possibly be improved through linker sequence optimizations to better pair V_H and V_L chains. However, this is beyond the scope of our research and supports our claim that evaluating nanobodies in a CAR context provides a more straightforward approach, owing to their monomeric nature. Moreover, nanobodies confer the additional opportunity to be used as diagnostic tools, by transforming them into imaging tracers.[28] The radiolabeled B7-H3 nanobody showed potent in vivo tumor targeting and is therefore considered a potential candidate for “theranostic” approaches. Proceeding to in vivo evaluation of the B7-H3 nanoCAR-T cell therapy, we observed that while the nanoCAR-T cells showed antitumor function against xenografted B7-H3^{pos} cells, the therapy was associated with a limiting toxicity. While the exact mechanism behind this toxicity remains to be fully elucidated, we suggest a role for on-target, off-tumor toxicity, induced by the B7-H3 nanoCAR’s reactivity against B7-H3 expressing healthy mouse tissue as a potential cause.

Considering the high sequence homology between human and mouse B7-H3, cross-reactivity of the nanobody was expected.[21] However, limited reports exist on expression patterns of mouse B7-H3 in healthy tissues as well as on tumor cells.[41–43] Based on these, and given the strong conservation of the B7-H3 molecule through evolution, we might consider that expression patterns in mice may be similar to those in humans where only low, heterogenous expression is observed in normal tissue.[21 44] A diffuse, rather than focal distribution of B7-H3 on normal mouse tissue is also in line with imaging and ex vivo biodistribution experiments in which B7-H3 radiolabeled nanobodies showed no significant SPECT/CT signal or uptake in any tissue, except for B7-H3^{pos} tumors.

Cross-reactivity of the B7-H3 nanobody towards cell-expressed mouse B7-H3 was confirmed using the mouse B7-H3-overexpressing CT26 cell line. Moreover, the B7-H3 nanoCARs ability to induce CAR signaling and T cell activation on recognition of low-level endogenous mouse B7-H3 was shown using wild-type B16 and CT26 cells and primary spleen and bone marrow cells, indicating that in

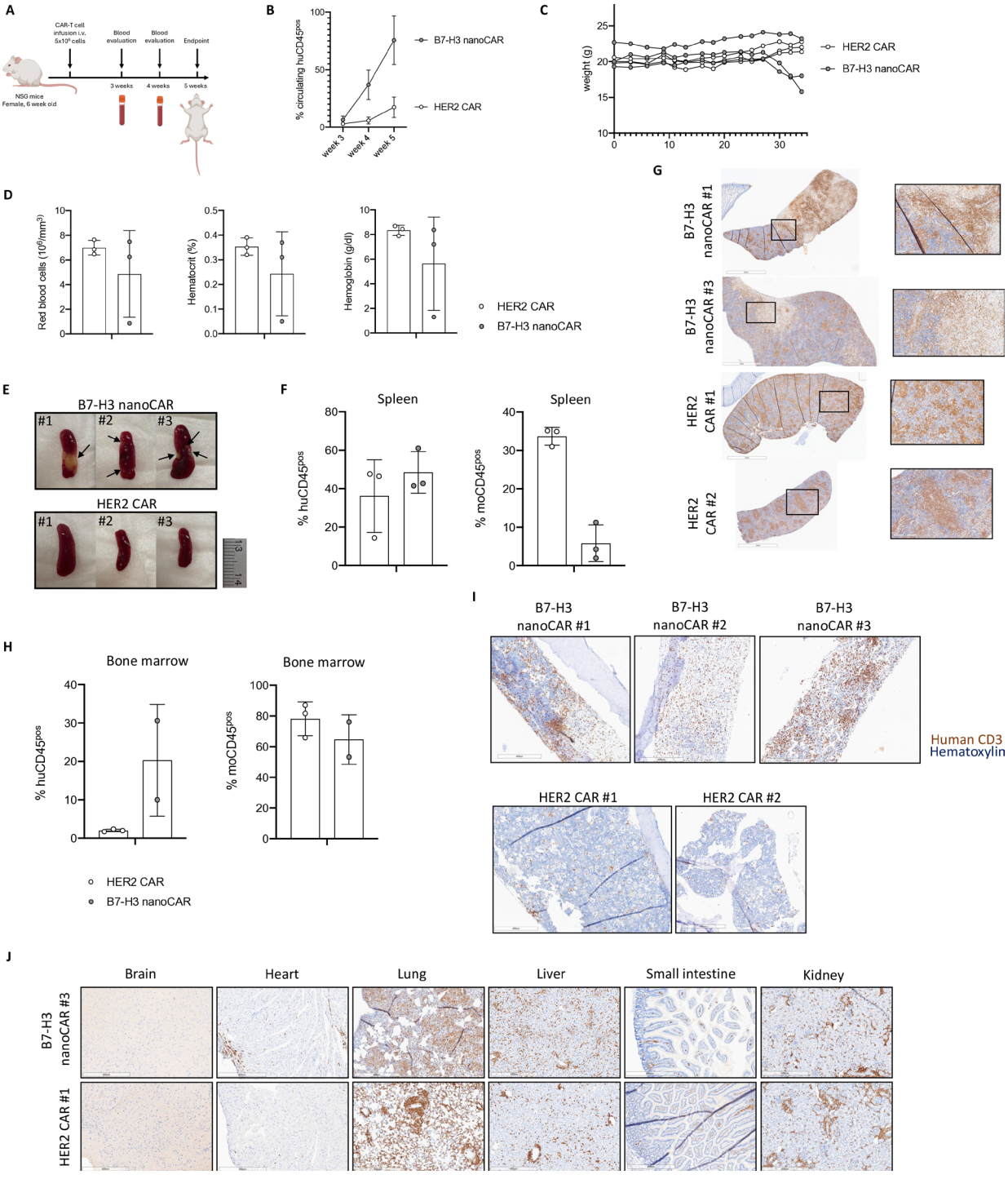

Figure 7 Reactivity of B7-H3 nanoCAR-T cells in non-tumor-bearing mice confirm the occurrence of on-target, off-tumor toxicity. (A) Graphical overview of in vivo experimental set-up. (B) Flow cytometry data of blood from mice, processed at 3, 4 and 5 weeks of CAR-T cell treatment, showing % of circulating human CD45 cells gated within all living blood cells. (C) Weight curves over time. (D) Hematological analysis of blood after 5 weeks of B7-H3 nanoCAR or HER2-CAR therapy evaluating red blood cell, hemoglobin and hematocrit levels as determined by the scil Vet abc Plus. (E) Images of spleens dissected from mice after 5 weeks of B7-H3 nanoCAR or HER2-CAR therapy. (F) Flow cytometry data of spleens from mice, processed at 5 weeks of CAR-T cell treatment, showing % of human and mouse CD45 cells gated within all living spleen cells (G) Immunohistochemical staining of spleens from the indicated mice, assessing CAR-T infiltration based on human CD3 staining. (H) Flow cytometry data of bone marrow cells from mice, processed at 5 weeks of CAR-T cell treatment, showing % of human and mouse CD45 cells gated within all living bone marrow cells. (I) Immunohistochemical staining of femurs from the indicated mice, assessing CAR-T infiltration based on human CD3 staining. (J) Representative Immunohistochemical staining of brain, heart, lung, liver, small intestine and kidney of mice with human CD3 antibody to detect CAR-T infiltration. Data represent mean±SD n=3 mice per group. B7-H3, B7 homolog 3; CAR, chimeric antigen receptor; HER2, human epidermal growth factor receptor 2; i.v., intravenously; nanoCAR, nanobody-based chimeric antigen receptor.

vivo too, the B7-H3 nanoCAR might have reacted against low-level B7-H3 expression on normal mouse tissue, causing the observed toxicity. As no toxicity was observed with HER2-targeting CAR-T cells in the tumor-bearing mouse model, we argue that the reaction is B7-H3-driven, rather than a result of GVHD, which usually manifests later and with different symptoms, in PBMC-humanized mouse models.[45] In addition, since the reactivity of B7-H3 nanoCAR-T cells—judged by weight loss, increased blood circulation of huCD45^{pos} cells, splenic toxicity and bone marrow involvement—occurred independent of tumor engraftment in non-tumor-bearing mice, toxicity was considered on-target, off-tumor. Based on our results, off-tumor reactivity seems to involve targeting moCD45^{pos} cell populations in the spleen and bone marrow, which is in line with a recent study reporting on B7-H3 expression on hematopoietic stem and progenitor cells.[46] In this regard, the in vivo xenograft model employed in our study poses limitations as it lacks a fully competent immune system and its subsets.[47] Performing experiments in an immunocompetent mouse model could further help to identify the extent to which these findings on on-target, off-tumor toxicity would translate to a human situation.

In contrast to the B7-H3 nanoCAR, the scFvCAR did not induce T cell activation on encounter with B7-H3-expressing mouse cells in the reporter T cell assay. In line with this, no other studies using B7-H3 scFvCAR-T cells have reported on B7-H3-targeted CAR-related toxicity in mice. This could be explained by the fact that these CARs are designed with scFvs derived from human B7-H3 antibodies. It has been reported that human B7-H3 antibodies counterintuitively do not recognize mouse B7-H3 when endogenously expressed by mouse cells, despite the high sequence homology.[21] The reason for this is reported to be due to differences in glycosylation patterns, likely disrupting antibody binding sites, rendering these human-B7-H3 scFvCARs unable to recognize endogenously expressed mouse B7-H3.[21] Nanobodies have been reported to have a higher propensity to bind hidden epitopes.[48] Therefore, while the scFvCAR, which is derived from a human antibody, does not, the nanoCAR used in this study most likely binds to an epitope that is only mildly or entirely unaffected by mouse glycosylation patterns.

While efforts have been made to predict the safety of new B7-H3 CAR-T cell products, most studies fail to report on CARs targeting mouse B7-H3 with similar affinity as its human counterpart. A study reporting on the evaluation of a cross-reactive B7-H3 CAR - designed with a different scFv (376.96)—reports on the absence of toxicity in mouse models.[43] However, affinity towards mouse B7-H3 (2340 nM) in their study is shown to be more than 100-fold weaker than in humans (18.5 nM) and is therefore most likely less sensitive towards low-level expression of mouse B7-H3.[43] Accordingly, another recent study evaluating B7-H3 nanoCAR-T cells in the context of solid tumors reports on the absence of toxicity in a syngeneic mouse model.[46] Here, the authors selected a nanobody with intermediate binding capacity (30.4 nM K_D to human B7-H3) to avoid on-target, off-tumor toxicity, but since affinity towards mouse B7-H3 strongly differs (473 nM K_D), it is difficult to predict sensitivity to off-tumor human B7-H3 expression. This is in contrast to our study where the affinity towards mouse (10 nM) and human (14.5 nM) proteins are highly similar.

Another recent study evaluating B7-H3 nanoCAR-T cells in the context of pancreatic ductal adenocarcinoma and metastatic neuroblastoma reports on the absence of toxicity in NSG mice.[49] This could be explained by the difference in nanobodies with distinct characteristics. While the nanobodies in this study show cross-reactivity for soluble mouse B7-H3 antigen, no data is shown for binding to endogenously expressed mouse B7-H3 on cells. Moreover, affinity of the nanobodies was performed using fragment crystallizable region (Fc)-tailed nanobodies, conferring an expected overestimation of the factual K_D of monomeric nanobodies, through the avidity effect. Therefore, no fair comparison can be made with the affinity determined for the nanobody used in our study, since this was determined for the nanobody in monomeric form. In addition to affinity, CAR-expression levels (or valency) might differ between our studies, which in combination with target-antigen expression levels, determine the avidity or strength of the CAR-T cell:target cell interaction.[50] Affinity and valency of CAR molecules on CAR-T cells have been shown to influence sensitivity towards lower levels of target-antigen expression.[51] Indeed, affinity modulation has been described to tune CAR functionality.[26] More specifically, weakening this parameter has been described to be beneficial for CAR design in terms of differentiating between healthy tissue expressing low levels of antigen, and tumor tissue expressing high levels of antigen.[52]

Our findings contrast with the results of Haydar *et al*, reporting on mouse B7-H3 scFvCAR-T cells showing functionality without toxicity in an immunocompetent mouse model.[53] While the scFv's affinity is not specified, the Fab fragment it originates from has an affinity of 24 nM K_D,[41] a 2.4-fold difference from the nanobody used in this study's nanoCAR (10 nM). Assuming a similar 24 nM affinity for the scFv, this 2.4-fold difference is unlikely to explain the discrepancy in toxicity between our studies, suggesting other contributing factors. Potential variables include CAR delivery method and promotor used (influencing CAR expression levels), epitope location and hinge region (influencing immune synapse formation), and costimulatory domain (influencing levels and kinetics of activation).[26] Ultimately, CAR activity is determined by all these factors combined, making it difficult to isolate the influence of any single parameter when comparing CARs that vary in multiple domains.

Overall, with this preclinical study in an immunocompetent mouse model reporting on safety[53] and since no reports on toxicity concerns have been raised from clinical trials evaluating B7-H3 CAR-T cells so far, this toxicity is expected to be characteristic for this particular

nanobody and may be solved by weakening antigen-sensitivity through affinity modulation or selection of antigen-binding domains less active towards low B7-H3 expression, urging further evaluation of new B7-H3 CAR-T cell products.

In conclusion, this study highlights the potential benefit of B7-H3 nanoCAR-T cells for glioblastoma therapy in terms of design, functionality and by providing the possibility of an image-guided approach. However, in vivo toxicity following B7-H3 nanoCAR-T cell therapy observed in this study warrants caution when developing CARs sensitive to low-level antigen expression and highlights the importance of profound preclinical investigation in relevant in vivo models, preceding carefully designed clinical studies evaluating safety in humans.

Author affiliations
[1]Translational Oncology Research Center (TORC), Department of Biomedical Sciences, Laboratory for Molecular and Cellular Therapy (LMCT), Vrije Universiteit Brussel, Brussels, Belgium
[2]Department of Medical Imaging (MIMA), Molecular Imaging and Therapy (MITH) research group, Vrije Universiteit Brussel, Brussels, Belgium
[3]Department of Hematology, Cellular Therapy Laboratory, University Hospital Brussels, Universitair Ziekenhuis Brussel, Brussels, Belgium
[4]Translational Oncology Research Center (TORC), Department of Biomedical Sciences, Hematology and Immunology Research Team (HEIM), Vrije Universiteit Brussel, Brussels, Belgium
[5]Department of Medical Oncology, University Hospital Brussels, Universitair Ziekenhuis Brussel, Brussels, Belgium
[6]Translational Oncology Research Center (TORC), Department of Biomedical Sciences, Laboratory for Medical and Molecular Oncology (LMMO), Vrije Universiteit Brussel, Brussels, Belgium

Acknowledgements The authors would like to thank Jan De Jonge for his technical assistance in the nanobody production and characterization process and Kevin De Jonghe for assistance with the radioactive labeling of the nanobody for the in vivo imaging and ex vivo biodistribution studies performed at the In vivo Cellular and Molecular Imaging (ICMI) Core Facility of the Vrije Universiteit Brussel (VUB). Furthermore, Petra Roman and Elsy Vaeremans are acknowledged for their technical contribution to the cloning and plasmid production work, which was performed at the UMCOR Molecular Biology and Virus Production Core Facility (VUB). We further thank Yves Heremans, who performed the immunohistochemistry analysis of tissues and organs at the central Visual and Spatial Tissue Analysis (VSTA) Core Facility (VUB). Analysis of anemia was performed with the support of Conny Gysemans, Marc Packbier and Marijke Viaene of the Clinical and Experimental Endocrinology lab (Katholieke Universiteit Leuven). Part of this work has been presented on the ESGCT 30th Annual Congress In collaboration with SFTCG and NVGCT Brussels and published as abstract. Figures were created with BioRender.com.

Contributors KB is the guarantor. BN suggested studying B7-H3 in the context of glioblastoma. FM was responsible for most of the practical work conducted in this study, including methodology, data processing, analysis and visualization as well as draft writing. CNF was responsible for nanobody and scFv production and characterization (SPR), as well as for imaging experiments, which were supervised by ND. YDV, CG, RMA, and KZ shared their expertise on plasmid cloning, vector design, lentiviral vector production, cell transduction and T cell assays. ADB, IVR and DA were responsible for collecting and processing peripheral blood mononuclear cells. ST, YDV, ND and KB had a supervising and advisory function, both experimentally and on data interpretation and manuscript writing, as well as in the acquisition of project funding.

Funding The following authors are predoctoral research fellows of the Research Foundation Flanders (FWO-V): FM (1S68523N), CNF (1SB9724N), RMA (1S05020N), and KZ (1S61023N). CG received personal funding via Eutopia (0ZR3808BOF). Additional project funding was obtained via the VUB strategic research programs 50, 83 and 84, Fund Paul De Knop, the Koning Boudewijn Stichting—Fund Catharina Weekers (2022-J1811380-E003), Research Foundation Flanders (project G028220N and EOS project 40007555) and the Scientific Fund Willy Gepts.

Competing interests No, there are no competing interests.

Patient consent for publication Not applicable.

Ethics approval This study involves human participants and was approved by Medical Ethical Committee of the UZ Brussel (BUN: 143201317905 and 1432023000220). Participants gave informed consent to participate in the study before taking part.

Provenance and peer review Not commissioned; externally peer reviewed.

Data availability statement Data are available upon reasonable request. All data relevant to the study are included in the article or uploaded as supplementary information.

ORCID iDs
Fien Meeus http://orcid.org/0000-0002-5866-2002
Cleo Goyvaerts http://orcid.org/0000-0002-1725-7772
Sandra Tuyaerts http://orcid.org/0000-0003-1255-8071
Nick Devoogdt http://orcid.org/0000-0001-9220-4833

REFERENCES

1 Tan AC, Ashley DM, López GY, *et al*. Management of glioblastoma: State of the art and future directions. *CA Cancer J Clin* 2020;70:299–312.
2 Verma A, Rafiq S. Chimeric Antigen Receptor (CAR) T Cell Therapy for Glioblastoma. *Cancer Treat Res* 2022;183:161–84.
3 Medikonda R, Dunn G, Rahman M, *et al*. A review of glioblastoma immunotherapy. *J Neurooncol* 2021;151:41–53.
4 Lim M, Xia Y, Bettegowda C, *et al*. Current state of immunotherapy for glioblastoma. *Nat Rev Clin Oncol* 2018;15:422–42.
5 Louveau A, Herz J, Alme MN, *et al*. CNS lymphatic drainage and neuroinflammation are regulated by meningeal lymphatic vasculature. *Nat Neurosci* 2018;21:1380–91.
6 Pombo Antunes AR, Scheyltjens I, Lodi F, *et al*. Single-cell profiling of myeloid cells in glioblastoma across species and disease stage reveals macrophage competition and specialization. *Nat Neurosci* 2021;24:595–610.
7 Duerinck J, Schwarze JK, Awada G, *et al*. Intracerebral administration of CTLA-4 and PD-1 immune checkpoint blocking monoclonal antibodies in patients with recurrent glioblastoma: a phase I clinical trial. *J Immunother Cancer* 2021;9:e002296.
8 Duerinck J, Tuyaerts S, Movahedi K, *et al*. Overcoming the immune suppressive nature of glioblastoma by leveraging the surgical intervention - current status and future perspectives. *Front Immunol* 2023;14:1183641.
9 Pombo Antunes AR, Scheyltjens I, Duerinck J, *et al*. Understanding the glioblastoma immune microenvironment as basis for the development of new immunotherapeutic strategies. *Elife* 2020;9:e52176.
10 June CH, Sadelain M. Chimeric Antigen Receptor Therapy. *N Engl J Med* 2018;379:64–73.
11 Majzner RG, Ramakrishna S, Yeom KW, *et al*. GD2-CAR T cell therapy for H3K27M-mutated diffuse midline gliomas. *Nat New Biol* 2022;603:934–41.
12 O'Rourke DM, Nasrallah MP, Desai A, *et al*. A single dose of peripherally infused EGFRvIII-directed CAR T cells mediates antigen

loss and induces adaptive resistance in patients with recurrent glioblastoma. *Sci Transl Med* 2017;9:eaaa0984.
13 Durgin JS, Henderson F Jr, Nasrallah MP, *et al*. Case Report: Prolonged Survival Following EGFRvIII CAR T Cell Treatment for Recurrent Glioblastoma. *Front Oncol* 2021;11:669071.
14 Ahmed N, Brawley V, Hegde M, *et al*. HER2-Specific Chimeric Antigen Receptor-Modified Virus-Specific T Cells for Progressive Glioblastoma: A Phase 1 Dose-Escalation Trial. *JAMA Oncol* 2017;3:1094–101.
15 Brown CE, Badie B, Barish ME, *et al*. Bioactivity and Safety of IL13Rα2-Redirected Chimeric Antigen Receptor CD8+ T Cells in Patients with Recurrent Glioblastoma. *Clin Cancer Res* 2015;21:4062–72.
16 Lin Q, Ba T, Ho J, *et al*. First-in-Human Trial of EphA2-Redirected CAR T-Cells in Patients With Recurrent Glioblastoma: A Preliminary Report of Three Cases at the Starting Dose. *Front Oncol* 2021;11:694941.
17 Brown CE, Alizadeh D, Starr R, *et al*. Regression of Glioblastoma after Chimeric Antigen Receptor T-Cell Therapy. *N Engl J Med* 2016;375:2561–9.
18 Rafiq S, Hackett CS, Brentjens RJ. Engineering strategies to overcome the current roadblocks in CAR T cell therapy. *Nat Rev Clin Oncol* 2020;17:147–67.
19 Majzner RG, Theruvath JL, Nellan A, *et al*. CAR T Cells Targeting B7-H3, a Pan-Cancer Antigen, Demonstrate Potent Preclinical Activity Against Pediatric Solid Tumors and Brain Tumors. *Clin Cancer Res* 2019;25:2560–74.
20 Zhou WT, Jin WL. B7-H3/CD276: An Emerging Cancer Immunotherapy. *Front Immunol* 2021;12:701006.
21 Kontos F, Michelakos T, Kurokawa T, *et al*. B7-H3: An Attractive Target for Antibody-based Immunotherapy. *Clin Cancer Res* 2021;27:1227–35.
22 Sun M, Richards S, Prasad DVR, *et al*. Characterization of mouse and human B7-H3 genes. *J Immunol* 2002;168:6294–7.
23 Getu AA, Tigabu A, Zhou M, *et al*. New frontiers in immune checkpoint B7-H3 (CD276) research and drug development. *Mol Cancer* 2023;22:43.
24 Son Y, Kwon SM, Cho JY. CD276 (B7-H3) Maintains Proliferation and Regulates Differentiation in Angiogenic Function in Late Endothelial Progenitor Cells. *Stem Cells* 2019;37:382–94.
25 Tang X, Wang Y, Huang J, *et al*. Administration of B7-H3 targeted chimeric antigen receptor-T cells induce regression of glioblastoma. *Signal Transduct Target Ther* 2021;6:125.
26 Hanssens H, Meeus F, De Veirman K, *et al*. The antigen-binding moiety in the driver's seat of CARs. *Med Res Rev* 2022;42:306–42.
27 Ackaert C, Smiejkowska N, Xavier C, *et al*. Immunogenicity Risk Profile of Nanobodies. *Front Immunol* 2021;12:632687.
28 Lecocq Q, De Vlaeminck Y, Hanssens H, *et al*. Theranostics in immuno-oncology using nanobody derivatives. *Theranostics* 2019;9:7772–91.
29 Awad RM, Meeus F, Ceuppens H, *et al*. Emerging applications of nanobodies in cancer therapy. *Int Rev Cell Mol Biol* 2022;369:143–99.
30 DuBridge R, Vinogradova M, Zhu Y. InventorsCoexpression and purification method of conditionally-activated binding proteins. 2020.
31 Lemaire M, D'Huyvetter M, Lahoutte T, *et al*. Imaging and radioimmunotherapy of multiple myeloma with anti-idiotypic Nanobodies. *Leukemia* 2014;28:444–7.
32 Carter P, Presta L, Gorman CM, *et al*. Humanization of an anti-p185HER2 antibody for human cancer therapy. *Proc Natl Acad Sci U S A* 1992;89:4285–9.
33 De Vlaeminck YD, Bonelli S, Awad RM, *et al*. Targeting Neuropilin-1 with Nanobodies Reduces Colorectal Carcinoma Development. *Cancers (Basel)* 2020;12:3582.
34 De Ridder K, Tung N, Werle J-T, *et al*. Novel 3D Lung Tumor Spheroids for Oncoimmunological Assays. *Adv NanoBiomed Res* 2022;2.
35 Webster B, Xiong Y, Hu P, *et al*. Self-driving armored CAR-T cells overcome a suppressive milieu and eradicate CD19+ Raji lymphoma in preclinical models. *Mol Ther* 2021;29:2691–706.
36 Vincke C, Gutiérrez C, Wernery U, *et al*. Generation of single domain antibody fragments derived from camelids and generation of manifold constructs. *Methods Mol Biol* 2012;907:145–76.
37 Vaneycken I, Devoogdt N, Van Gassen N, *et al*. Preclinical screening of anti-HER2 nanobodies for molecular imaging of breast cancer. *FASEB J* 2011;25:2433–46.
38 Kirsten DR, Navpreet T, Jan-Timon W, *et al*. Novel 3d lung tumor spheroids for oncoimmunological assays. *Advanced Nanobiomed Research*; 2021.
39 Xavier C, Devoogdt N, Hernot S, *et al*. mTc: a practical guide. *Methods Mol Biol* 2012;911:485–90.
40 Zeven K, De Groof TWM, Ceuppens H, *et al*. Development and evaluation of nanobody tracers for noninvasive nuclear imaging of the immune-checkpoint TIGIT. *Front Immunol* 2023;14:1268900.
41 Seaman S, Zhu Z, Saha S, *et al*. Eradication of Tumors through Simultaneous Ablation of CD276/B7-H3-Positive Tumor Cells and Tumor Vasculature. *Cancer Cell* 2017;31:501–15.
42 Khan KA, Kerbel RS. A CD276 Antibody Guided Missile with One Warhead and Two Targets: The Tumor and Its Vasculature. *Cancer Cell* 2017;31:469–71.
43 Du H, Hirabayashi K, Ahn S, *et al*. Antitumor Responses in the Absence of Toxicity in Solid Tumors by Targeting B7-H3 via Chimeric Antigen Receptor T Cells. *Cancer Cell* 2019;35:221–37.
44 Wang L, Kang FB, Shan BE. B7-H3-mediated tumor immunology: Friend or foe? *Int J Cancer* 2014;134:2764–71.
45 Elhage A, Sligar C, Cuthbertson P, *et al*. Insights into mechanisms of graft-versus-host disease through humanised mouse models. *Biosci Rep* 2022;42:BSR20211986.
46 Yeo SP, Kua L, Tan JW, *et al*. B7-H3-Targeting Chimeric Antigen Receptors Epstein-Barr Virus-specific T Cells Provides a Tumor Agnostic Off-The-Shelf Therapy Against B7-H3-positive Solid Tumors. *Cancer Res Commun* 2024;4:1410–29.
47 Duncan BB, Dunbar CE, Ishii K. Applying a clinical lens to animal models of CAR-T cell therapies. *Mol Ther Methods Clin Dev* 2022;27:17–31.
48 Hassanzadeh-Ghassabeh G, Devoogdt N, De Pauw P, *et al*. Nanobodies and their potential applications. *Nanomed (Lond)* 2013;8:1013–26.
49 Li D, Wang R, Liang T, *et al*. Camel nanobody-based B7-H3 CAR-T cells show high efficacy against large solid tumours. *Nat Commun* 2023;14:5920.
50 Jayaraman J, Mellody MP, Hou AJ, *et al*. CAR-T design: Elements and their synergistic function. *EBioMedicine* 2020;58:102931.
51 Harrer DC, Li SS, Kaljanac M, *et al*. Fine-tuning the antigen sensitivity of CAR T cells: emerging strategies and current challenges. *Front Immunol* 2023;14:1321596.
52 Duan Y, Chen R, Huang Y, *et al*. Tuning the ignition of CAR: optimizing the affinity of scFv to improve CAR-T therapy. *Cell Mol Life Sci* 2021;79:14.
53 Haydar D, Houke H, Chiang J, *et al*. Cell-surface antigen profiling of pediatric brain tumors: B7-H3 is consistently expressed and can be targeted via local or systemic CAR T-cell delivery. *Neuro Oncol* 2021;23:999–1011.